Reliability-Oriented Adaptive Switching Frequency Scheme for Modular Multilevel Converters

Yi ZHANG, Yaqian ZHANG, and Zhongxu WANG

***Abstract*—Modular multilevel converters (MMCs) are widely utilized in medium voltage grid-connected applications, typically employing carrier phase shift modulation. However, the high switching frequency associated with this modulation scheme often increases power losses and thermal stress on semiconductor devices, negatively impacting their efficiency and reliability. In this paper, we propose an adaptive switching frequency scheme that divides the carrier frequency into several discrete zones based on load conditions. Through analytical evaluation of the carrier frequency, our proposed method optimizes it to meet power quality and capacitor voltage ripple requirements, effectively reducing power losses and thermal stress. A simulation case study based on a 15-MVA MMC demonstrates a remarkable 21% reduction in annual power losses and a 12% reduction in annual damage, thereby improving efficiency and reliability. Additionally, experimental measurements conducted on a 15-kW downscale platform validate around 10% reduction in power losses while fulfilling power quality and capacitor voltage ripple requirements.**

***Index Terms*—Efficiency, modular multilevel converters (MMC), reliability, switching frequency, thermal stress.**

I. INTRODUCTION

MODULAR multilevel converters (MMC) have advantages in medium-voltage (MV) applications such as scalability, low d*v*/d*t* [1], [2], etc. However, the reliability of MMC is a critical aspect to consider, primarily due to a large number of insulated-gate bipolar transistors (IGBTs) [3], which are exposed to severe thermal stresses [4].

To enhance the reliability of the MMC, various methods have been proposed to manage thermal stress [5], [6]. For instance, in [7], [8], temperature balancing control techniques are introduced to alleviate thermal imbalances among different sub-modules (SMs). Another approach presented in [9] involves regulating the dc offset of modulation waves to achieve balanced thermal stress on the upper and lower power devices within the same SM. However, a common challenge faced by these methods is the requirement of accurately estimating junction temperature as feedback to regulate thermal stress, which relies on precise modeling of power losses and thermal parameters [10]. Additionally, these modeling parameters are difficult to obtain accurately and are subject to uncertainties in practice, such as degradation, operational conditions, and system-level thermal couplings [3].

In contrast to actively controlling the junction temperature, a target of reducing power losses are more tangible for practical systems. By focusing on adjusting key quantities that impact power losses, the accurate estimation of power losses and thermal stresses are eliminated. Power losses of the IGBTs primarily consist of conduction and switching losses [11], [12]. A typical approach is thus to suppress the harmonic components in the arm current [13]–[15] to reduce conduction losses, but these methods can lead to increased capacitor voltage ripples [16]. Another perspective is to focus on reducing switching losses, which constitute a larger proportion of total power losses, particularly in the MV applications utilizing carrier-phase shift pulse width modulation (CPSPWM) [17], [18]. Lowering the carrier frequency can reduce switching losses, but it may also have implications for other performance metrics, such as voltage balancing, SM voltage ripple amplitude, and Total Harmonic Distortion (THD) of ac current [19]–[21]. Therefore, the challenge lies in optimizing between reducing switching power losses and maintaining specific performance requirements for the MMC.

To simultaneously reduce power losses and meet specific performance requirements, such as THD and maximum allowable capacitor voltage ripple, this paper proposes an adaptive switching frequency scheme for the MMC. The scheme utilizes an analytical model to establish the relationship between the carrier frequency and its impact on MMC performance metrics under different operating conditions. By setting desired THD and voltage ripple limits, the converter power loading inputs are divided into several discrete zones with optimal carrier frequencies. The effectiveness of the proposed approach is validated through simulation based on a oneyear mission profile and experiments on a down-scale MMC prototype. Comparative analysis with the conventional fixed carrier frequency modulation method demonstrates that the adaptive frequency approach not only meets the operational performance requirements of the MMC but also improves its efficiency and reliability.

Manuscript received May 8, 2023; revised July 10, 2023 and August 18, 2023; accepted August 22, 2023. Date of publication March 30, 2024; date of current version September 4, 2023. This work was supported by Independent Research Fund Denmark with the grant number 1031-00024B. *(Corresponding author: Yaqian Zhang.)*

Yi Zhang is with AAU Energy, Aalborg University, Pontoppidanstraede 101 Address (Cont'd) Aalborg, Aalborg, Denmark (e-mail: yiz@ieee.org).

Yaqian Zhang is with Southeast University, Nanjing, Jiangsu 210096, China (e-mail: yaqianzhang83@seu.edu.cn).

Z. Wang is with Nexperia BV, Nijmegen 6534 AB, UK (e-mail: zhongxu2020@gmail.com).

Digital Object Identifier 10.24295/CPSSTPEA.2023.00039

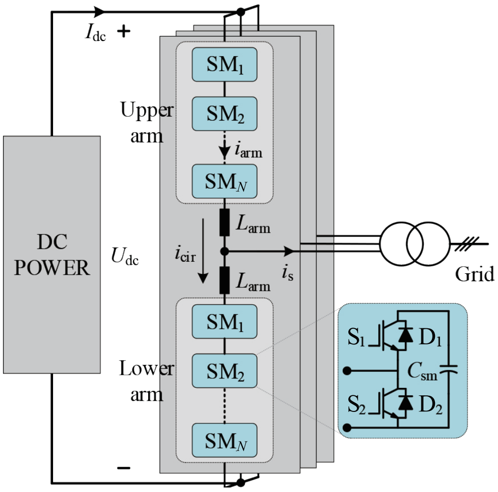

Fig. 1. A typical grid-connected three-phase MMC system.

II. Operating Principles of Modular Multilevel Converters

A. System Description of MMC

Fig. 1 illustrates a general three-phase grid-connected MMC topology with symmetric upper and lower arms in each phase. In each arm, there is one arm inductor cascaded with N identical half-bridge submodules (HBSMs). C_{sm} represents the SM capacitance. In a phase, the arm currents are expressed as

$$\begin{cases} i_p = i_{cir} + \dfrac{i_s}{2} = \dfrac{I_{dc}}{3} + \dfrac{I_s}{2}\sin(\omega_1 t+\varphi_1) \\ i_n = i_{cir} - \dfrac{i_s}{2} = \dfrac{I_{dc}}{3} - \dfrac{I_s}{2}\sin(\omega_1 t+\varphi_1) \end{cases} \tag{1}$$

where $i_{p/n}$ represents the upper or lower arm currents, I_{dc} is the dc current, and i_s is the ac output current with an amplitude of I_s. i_{cir} is the circulating current. ω_1 denotes the angular frequency and φ_1 is the initial angle.

The upper and lower arm voltages (u_p and u_n) are

$$\begin{cases} u_p = \dfrac{U_{dc}}{2} - u_o = \dfrac{U_{dc}}{2}\left[1 - m\sin(\omega_1 t)\right] \\ u_n = \dfrac{U_{dc}}{2} + u_o = \dfrac{U_{dc}}{2}\left[1 + m\sin(\omega_1 t)\right] \end{cases} \tag{2}$$

where U_{dc} denotes the dc voltage. m represents the modulation index which is defined as $U_m/(U_{dc}/2)$. U_m is the ac output voltage amplitude. The dc voltage has $U_{dc} = NU_C$, in which U_C is the SM nominal voltage.

Since the arm voltage is evenly distributed among N SMs, the output voltage of each SM is normalized as

$$\begin{cases} u_{p,ref} = \dfrac{1}{2}\left[1 - m\cos(\omega_1 t)\right] \\ u_{n,ref} = \dfrac{1}{2}\left[1 + m\cos(\omega_1 t)\right] \end{cases} \tag{3}$$

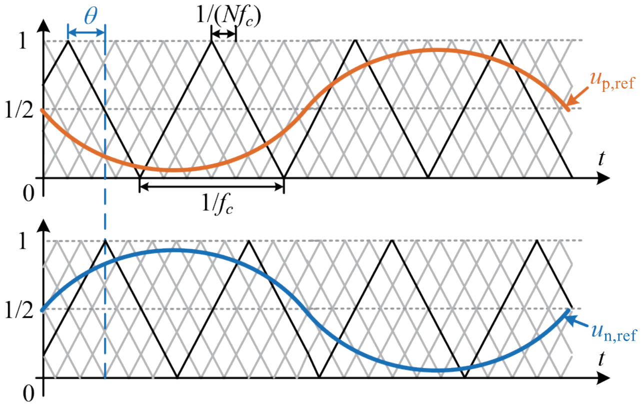

Fig. 2. CPS-PWM modulation of MMC.

where $u_{p,ref}$, and $u_{n,ref}$ are the reference SM output voltage in the upper and lower arms, respectively.

B. Conventional CPS-PWM Modulation

In MV MMCs, the CPS-PWM modulation is commonly used to achieve high output current quality [17]. Fig. 2 illustrates the principle of the modulation wave (refers to (3)), where an angular displacement of $2\pi/N$ is defined for N carrier waves for each SM. Additionally, an angular displacement, denoted as θ, also exists between the upper and lower arm carrier waves, whose frequency and angular frequency are defined as f_c and ω_c, and shared by all SMs.

Typically, the carrier waves, including the carrier frequency and the phase displacement, are fixed for an MMC system, which is however not always optimal given varied operation conditions. This paper will investigate the option of changing the carrier frequency to reduce power losses and improve the reliability of the MMC system.

III. Proposed Adaptive Frequency Scheme

This section presents an adaptive carrier frequency scheme for the MMC that enhances operational efficiency while meeting specific requirements under varying power levels. The scheme primarily focuses on two critical aspects: output current THD and SM capacitor voltage ripple. Both of these performance metrics are significantly influenced by the carrier frequency adjustment. The proposed approach aims to dynamically adapt the carrier frequency according to the load conditions, ensuring that desired targets for capacitor voltage ripple and THD are achieved simultaneously.

A. The Relationship Between Carrier Frequency and THD

A Fourier series is employed to investigate the relationship between the carrier frequency and THD of the MMC [17]. $u_{s,f/h}$, $i_{s,f/h}$, and $u_{grid,f/h}$ represent the fundamental component and harmonic component of the ac voltage, ac current, and the grid voltage, respectively. The output voltage of the SMs in the upper and lower arms can be expressed as

$$\begin{cases} u_{\mathrm{p},i}=\dfrac{U_{\mathrm{dc}}}{2N}-\dfrac{mU_{\mathrm{dc}}}{2N}\cos(\omega_1 t)+ \\ \displaystyle\sum_{\mathrm{a}=1}^{\infty}\sum_{\mathrm{b}=-\infty}^{\infty}\frac{2U_{\mathrm{dc}}}{a\pi N}\sin\left[\frac{(\mathrm{a+b})\pi}{2}\right]\times J_{\mathrm{b}}\left(\frac{ma\pi}{2}\right) \\ \cos\left\{\mathrm{a}\left[\omega_{\mathrm{c}}t+\theta+(i-1)\dfrac{2\pi}{N}\right]+b\omega_1 t+b\pi\right\} \\ u_{\mathrm{n},i}=\dfrac{U_{\mathrm{dc}}}{2N}+\dfrac{mU_{\mathrm{dc}}}{2N}\cos(\omega_1 t)+ \\ \displaystyle\sum_{\mathrm{a}=1}^{\infty}\sum_{\mathrm{b}=-\infty}^{\infty}\frac{2U_{\mathrm{dc}}}{a\pi N}\sin\left[\frac{(\mathrm{a+b})\pi}{2}\right]\times J_{\mathrm{b}}\left(\frac{ma\pi}{2}\right) \\ \cos\left\{\mathrm{a}\left[\omega_{\mathrm{c}}t+(i-1)\dfrac{2\pi}{N}\right]+b\omega_1 t\right\} \end{cases} \tag{4}$$

where $u_{\mathrm{p/n},i}$ is the i^{th} SM output voltage in the upper and lower arm; J_{b} is the first kind Bessel function with the a-th and b-th order harmonic components. Summing up all SMs, (2) is rewritten as

$$\begin{cases} u_{\mathrm{p}}=\dfrac{U_{\mathrm{dc}}}{2}-\dfrac{mU_{\mathrm{dc}}}{2}\cos(\omega_1 t)+ \\ \displaystyle\sum_{\mathrm{a}=1}^{\infty}\sum_{\mathrm{b}=-\infty}^{\infty}\frac{2U_{\mathrm{dc}}}{a\pi}\sin\left[\frac{(\mathrm{a+b})\pi}{2}\right]\times J_{\mathrm{b}}\left(\frac{ma\pi}{2}\right) \\ \cos\left\{\mathrm{a}\left[\omega_{\mathrm{c}}t+\theta+(i-1)\dfrac{2\pi}{N}\right]+b\omega_1 t+b\pi\right\} \\ u_{\mathrm{n}}=\dfrac{U_{\mathrm{dc}}}{2}+\dfrac{mU_{\mathrm{dc}}}{2}\cos(\omega_1 t)+ \\ \displaystyle\sum_{\mathrm{a}=1}^{\infty}\sum_{\mathrm{b}=-\infty}^{\infty}\frac{2U_{\mathrm{dc}}}{a\pi}\sin\left[\frac{(a+b)\pi}{2}\right]\times J_{\mathrm{b}}\left(\frac{ma\pi}{2}\right) \\ \cos\left\{\mathrm{a}\left[\omega_{\mathrm{c}}t+(i-1)\dfrac{2\pi}{N}\right]+b\omega_1 t\right\} \end{cases} \tag{5}$$

As a result, the ac voltage of MMC is given by

$$\begin{cases} u_{\mathrm{s}}=\dfrac{1}{2}(u_{\mathrm{n}}-u_{\mathrm{p}})=H(u_{\mathrm{s}})_{\mathrm{f}}\cdot\cos(\omega_1 t)+H(u_{\mathrm{s}})_{\mathrm{a,b}}\times \\ \cos\left[(Na\omega_{\mathrm{c}}+\mathrm{b}\omega_1)\mathrm{t}+\dfrac{Na\theta+b\pi-\pi}{2}\right] \\ H(u_{\mathrm{s}})_{\mathrm{f}}=\dfrac{mU_{\mathrm{dc}}}{2} \\ H(u_{\mathrm{s}})_{\mathrm{a,b}}=\dfrac{2U_{\mathrm{dc}}}{a\pi N}\sin\left[\dfrac{(Na+b)\pi}{2}\right]\times \\ J_{\mathrm{b}}\left(\dfrac{mNa\pi}{2}\right)\cos\left(\dfrac{Na\theta+b\pi-\pi}{2}\right) \end{cases} \tag{6}$$

where u_{s} is the ac voltage; $H(u_{\mathrm{s}})_{\mathrm{f}}$ is the amplitude of the fundamental component; $H(u_{\mathrm{s}})_{\mathrm{a,b}}$ is the harmonic components.

In a three-phase MMC system, the output power is

$$S=\frac{3}{2}H(u_{\mathrm{s}})_{\mathrm{f}}H(i_{\mathrm{s}})_{\mathrm{f}} \tag{7}$$

where S denotes the apparent power. $H(i_{\mathrm{s}})_{\mathrm{f}}$ is the fundamental component amplitude of the output current, which has

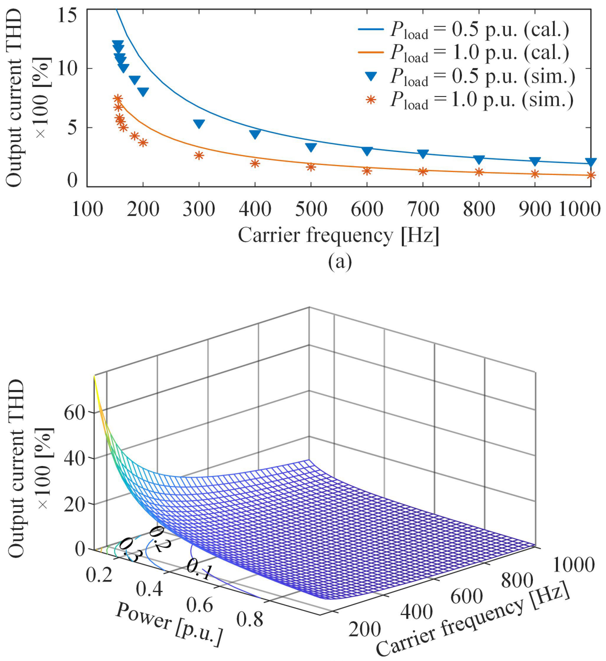

(a)

(b)

Fig. 3. Output current THD under different power loadings and carrier frequencies. (a) Analytical and simulation results under two loading conditions (cal.: calculated results by the proposed analytical model, sim.: simulation results based on parameters in Table I). (b) Impact of carrier frequency and power loading on the THD.

$$H(i_{\mathrm{s}})_{\mathrm{f}}=\frac{2S}{3H(u_{\mathrm{s}})_{\mathrm{f}}} \tag{8}$$

Under an ideal grid condition, the output current harmonics are driven by the corresponding harmonic components in u_{s}, which has an amplitude of

$$H(i_{\mathrm{s}})_{\mathrm{a,b}}=\frac{H(u_{\mathrm{s}})_{\mathrm{a,b}}}{\omega_{\mathrm{a,b}}(L_{\mathrm{arm}}/2+L_{\mathrm{grid}})} \tag{9}$$

where $H(i_{\mathrm{s}})_{\mathrm{a,b}}$ is the amplitude of a-th or b-th order harmonic components in the ac current. L_{arm} and L_{grid} are the arm and grid inductance, respectively. Combining (8) and (9), the output current THD can be derived as

$$THD(i_{\mathrm{s}})=\frac{\sqrt{\displaystyle\sum_{\mathrm{a}=1}^{\infty}\sum_{\mathrm{b}=-\infty}^{\infty}H(i_{\mathrm{s}})^{2}{}_{\mathrm{a,b}}}}{H(i_{\mathrm{s}})_{\mathrm{f}}} \tag{10}$$

Based on the analysis above, the relationship among power level, carrier frequency, and ac current THD can be depicted as in Fig. 3, where the current THD goes down as the carrier frequency increases given a constant power level. However, when the carrier frequency is fixed, the THD increases sharply under light load. For instance, to satisfy a standard THD requirement of 5% [21], the required carrier frequency is 200 Hz for P_{load} = 1.0 p.u., but it rises to 400 Hz for P_{load} = 0.5 p.u.. Thus, to limit the THD within 5%, the carrier frequencycan be adaptively adjusted by the following expression

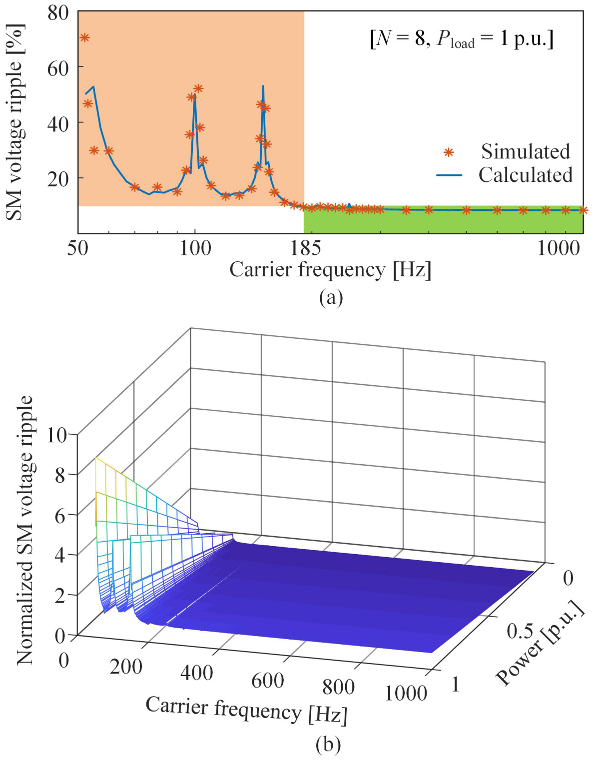

(a)

(b)

Fig. 4. Analytical model of SM voltage ripple. (a) Analytical and simulation results, where the orange region indicates the capacitor voltage ripple above 10% while the green region is below 10%. (b) Impact of carrier frequency and power loading on the capacitor voltage ripple.

$$\sqrt{\sum_{a=1}^{\infty}\sum_{b=-\infty}^{\infty} H(i_s)^2_{\text{a,b}}} = 5\%\times H(i_s)_{\text{f}} \tag{11}$$

B. The Relationship Between Carrier Frequency and Capacitor Voltage Ripple

According to [22], the SM capacitor voltage ripple can be derived as,

$$\begin{cases} u_{\text{cap,p},i} = U_{\text{sm}} + \dfrac{1}{C_{\text{sm}}}\displaystyle\int\left[\mathrm{A}\left(i_{\text{cir}}+\dfrac{1}{2}i_{\text{s}}\right)\right] \\ A = \dfrac{1}{2}-\dfrac{m}{2}\cos(\omega_1 t)+K_{\text{a,b}}\cos(\omega_{\text{a,b}}t+\alpha_{\text{p,a,b}}) \\ K_{\text{a,b}} = \displaystyle\sum_{a=1}^{\infty}\sum_{b=-\infty}^{\infty}\dfrac{2}{a\pi}\sin\left[\dfrac{(a+b)\pi}{2}\right]\times J_{\text{b}}\left(\dfrac{ma\pi}{2}\right) \\ \omega_{\text{a,b}} = a\omega_{\text{c}}+b\omega_1 \\ \alpha_{\text{p,a,b}} = a\theta+a(i-1)\dfrac{2\pi}{N}+b\pi \end{cases} \tag{12}$$

Its relationship with the carrier frequency and power level is illustrated in Fig. 4. The voltage ripple is limited to 10% and remains almost constant by keeping the carrier frequency higher than 185 Hz under the unity power loading in Fig. 4(a). With the decrease of the power level, the SM voltage ripple goes down under the same carrier frequency as shown in Fig. 4(b). This indicates that 185 Hz is sufficient for the MMC to maintain a 10% voltage ripple regardless of the power level.

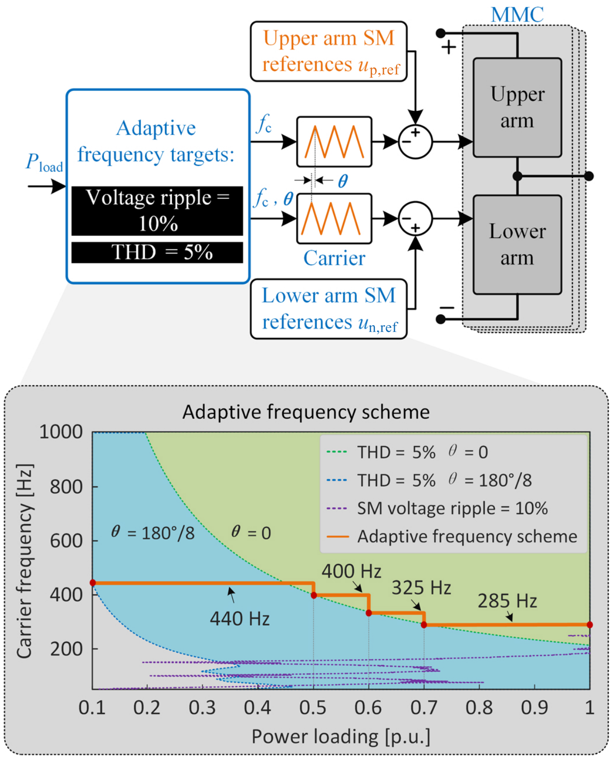

Fig. 5. Diagram of proposed adaptive frequency scheme and the result based on the case study of Table I. P_{load} is varied power level of the system.

TABLE I
MMC Parameters Used for Case Study

Parameter	Value	Parameter	Value
Power rating P	15 MVA	SM number per arm N	8
SM rated voltage U_{sm}	2.5 kV	SM capacitance C_{sm}	3.0 mF
DC-link voltage U_{dc}	20 kV	Arm inductance L_{arm}	4.1 mH
Power factor	1.0	Case temperature T_{c}	40 °C
Modulation index m	0.9		

C. Proposed Adaptive Switching Frequency Scheme

The detailed implementation of the adaptive switching frequency scheme is depicted in Fig. 5 based on a case study listed in Table I. The two performance requirements are to always limit 5% THD and 10% capacitor voltage ripple while adjusting carrier frequency.

Firstly, the power loading of the MMC is the input of this scheme. The required carrier frequency can be derived through offline calculation of (11) to achieve 5% THD under different power levels and yield the blue dashed line depicted in Fig. 5. Secondly, the capacitor voltage ripple is evaluated using (12), resulting in the purple dashed line.

Those three dashed lines give the selection boundary of carrier frequency, where the THD requirement takes precedence and requires a higher frequency. In order to avoid frequent adjustment of carrier frequency in practice, the

TABLE II

Curve Fitting Results of the Relationship Among Carrier Frequency, Junction Temperature, and Power Loading

$F\,(P_{\text{load}})$	a_1	a_2	a_3	$F\,(f_c)$	a_4	a_5
$\Delta T_{S_2@325\text{Hz}}$	1.211×10^{0}	6.345×10^{0}	0	$\Delta T_{S_2@0.5\text{pu}}$	0.607×10^{-2}	1.413×10^{0}
$\Delta T_{S_2@440\text{Hz}}$	1.109×10^{-1}	8.119×10^{0}	0	$\Delta T_{S_2@1\text{pu}}$	1.368×10^{-2}	3.119×10^{0}
$T_{\text{m\_}S_2@325\text{Hz}}$	5.480×10^{0}	3.456×10^{1}	4.0×10^{1}	$T_{\text{m\_}S_2@0.5\text{pu}}$	4.191×10^{-2}	4.459×10^{1}
$T_{\text{m\_}S_2@440\text{Hz}}$	5.386×10^{-2}	4.404×10^{1}	4.0×10^{1}	$T_{\text{m\_}S_2@1\text{pu}}$	8.824×10^{-2}	5.192×10^{1}
$P_{\text{loss}@325\text{Hz}}$	4.190×10^{2}	1.230×10^{5}	0	$P_{\text{loss}@0.5\text{pu}}$	1.131×10^{2}	1.150×10^{4}
$P_{\text{loss}@440\text{Hz}}$	3.777×10^{3}	9.650×10^{5}	0	$P_{\text{loss}@1\text{pu}}$	2.199×10^{2}	2.930×10^{4}

theoretically continuous carrier frequency is discretized into several levels based on power loading change of every 0.1 p.u., represented by the staircase lines in Fig. 5 for this case study.

IV. Comparison of the Proposed Method and Conventional Fixed Frequency Scheme

In this section, a comparative analysis is conducted between the proposed adaptive switching frequency scheme and the conventional fixed frequency scheme. The evaluation is performed on an MMC system connected to an offshore wind farm, using the converter system parameters specified in Table I. The assessment focuses on the reliability performance of the MMC over a one-year mission profile. The detailed evaluation process is in accordance with our previous work [3].

The evaluation process in this paper can be summarized into two aspects. Firstly, numerical relationships between power losses, thermal loading, power levels, and carrier frequency are established by fitting simulation results. This curve-fitting process allows us to quantify the impact of various factors on power losses and thermal stress. Secondly, based on these numerical relationships, an annual mission profile for the MMC system is utilized to compare the performance of the conventional and proposed switching frequency schemes.

A. Modeling of Power Losses and Thermal Stresses

To assess the long-term mission profile behavior of the MMC, numerical functions are needed to describe the relationship between power loss/thermal stress and the carrier frequency and power load, and it can be derived from simulation results shown in Fig. 6. Taking two carrier frequencies, 325 Hz and 440 Hz, as examples, the effects of carrier frequency and power loading on the junction temperature cycle amplitudes and the average value of four semiconductor devices (IGBTs S_1, S_2, and freewheeling diodes D_1, D_2) in an SM can be obtained and curve fitted by using the following polynomials:

$$\begin{cases} F(P_{\text{load}}) = a_1 P_{\text{load}}^2 + a_2 P_{\text{load}} + a_3 \\ F(f_c) = a_4 f_c + a_5 \end{cases} \tag{13}$$

where F represents the amplitude of the junction temperature cycle (ΔT), power loss (P_{loss}), or average junction temperature (T_{m}); a_i (i = 1...5) are the coefficients obtained from the curve fitting process. The specific values of a_i are listed in Table II.

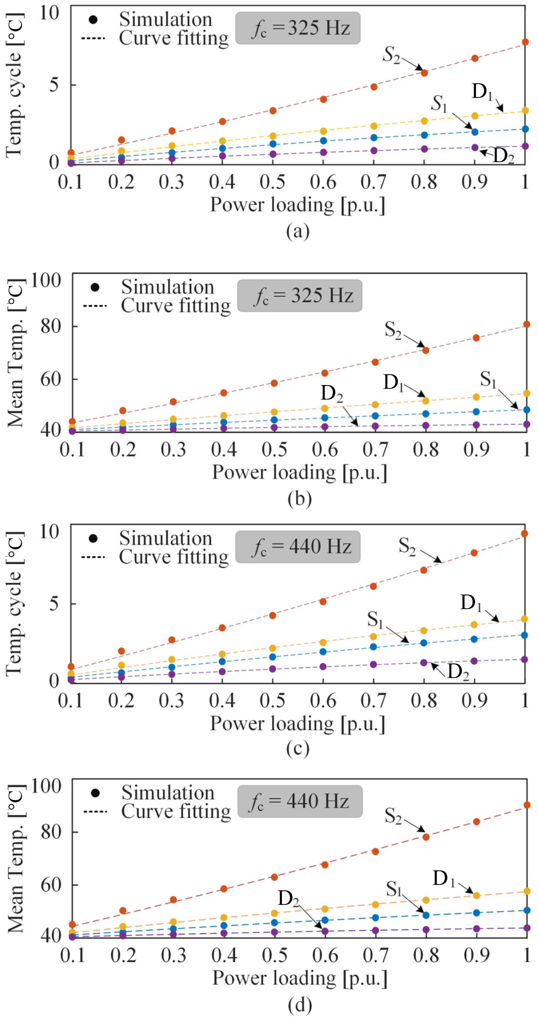

(a)

(b)

(c)

(d)

Fig. 6. Impact of power loading on the junction temperatures of the power devices. (a) Amplitude of junction temperature cycles and (b) mean junction temperatures at f_c = 325 Hz, (c) amplitude of junction temperature cycles and (d) mean junction temperatures at f_c = 440 Hz.

All these numerical relationships are based on normalized power loading. Considering the almost linear relationship between $F(x)$ and the carrier frequency and power loading, the following expression is derived:

$$F(P_{\text{load}}, f_c) = \frac{F(P_{\text{load}})_{@440\text{Hz}} - F(P_{\text{load}})_{@325\text{Hz}}}{440-325} \times (f_c - 325) + F(P_{\text{load}})_{@325\text{Hz}} \tag{14}$$

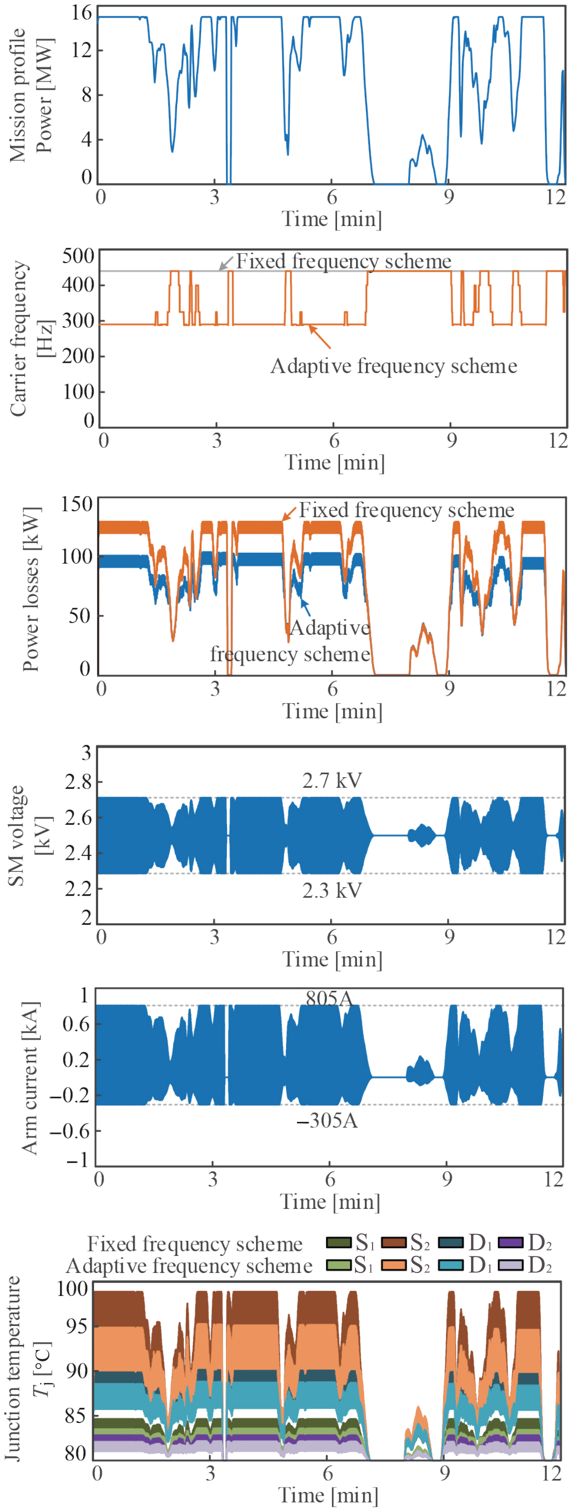

Fig. 7. Detailed mission profile evaluation for a 12-min varied loading condition.

where $F(P_{\text{load}})_{@325\text{Hz}}$ and $F(P_{\text{load}})_{@440\text{Hz}}$ are polynomial obtained by curve fitting under 325 Hz and 440 Hz.

B. Conversion from Mission Profile into Power Loss, Thermal Stress and Reliability Evaluation

Based on (14), the power loss and thermal stress of the devices can be fully evaluated for an annual mission profile. Fig. 7 demonstrates the detailed 12-min waveform out of the annual mission profile. The proposed adaptive frequency scheme helps reduce both the power losses and the junction temperature. Meanwhile, the SM capacitor voltages are still balanced with its voltage ripples within 10%. The annual

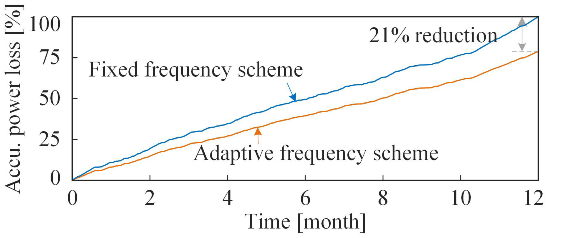

Fig. 8. Impact of the proposed method on the normalized accumulated power loss.

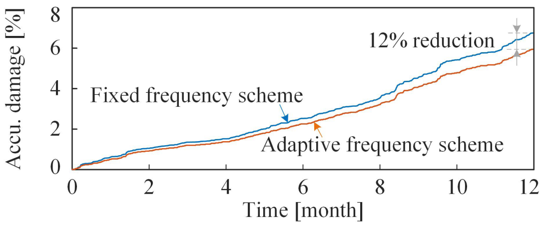

Fig. 9. Comparison of the accumulated damage between the fixed adaptive frequency schemes.

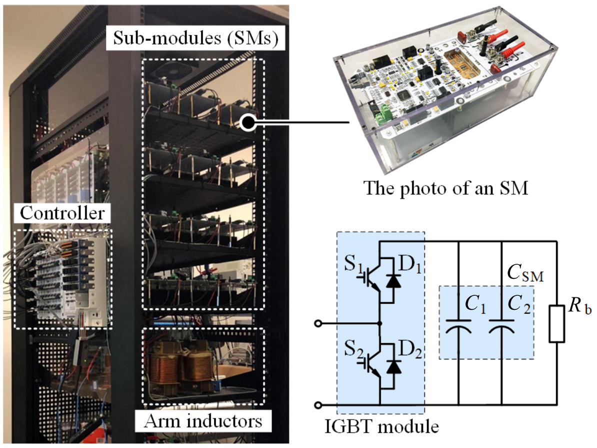

Fig. 10. Experimental prototype.

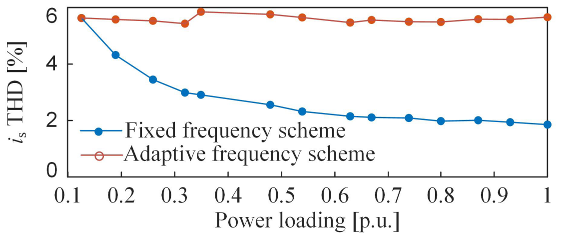

Fig. 11. Experimental output current THD.

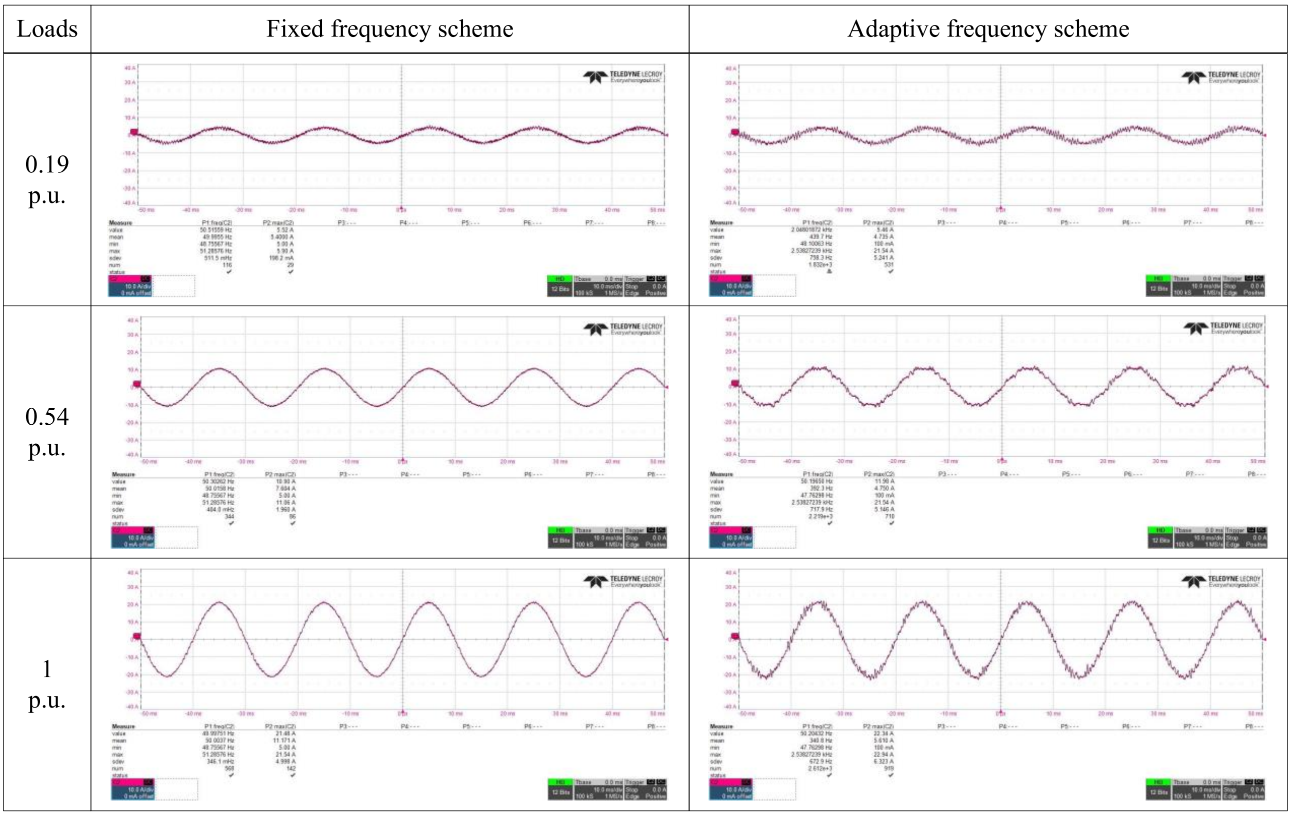

Fig. 12. Current waveforms under different loading conditions.

TABLE III
EXPERIMENTAL MMC PROTOTYPE PARAMETERS

Parameter	Value	Parameter	Value
Power rating P	15 kV	SM number per arm N	4
DC-link voltage U_{dc}	900 V	SM voltage U_{sm}	225 V
Arm inductance L_{arm}	4 mH	SM capacitance C_{sm}	1.5 mF
Modulation index m	0.17	Ambient temperature T_{a}	24 °C

accumulated power losses are shown in Fig. 8, which achieves a 21% reduction for the proposed method.

To evaluate the reliability, the below lifetime model is used

$$N_{\mathrm{f}}=A\left(\triangle T_{\mathrm{j}}\right)^{\alpha}\cdot\exp\left(\frac{E_{\mathrm{a}}}{k_{\mathrm{b}}T_{\mathrm{jm}}}\right) \tag{15}$$

where N_{f} represents the number of cycle life under a condition with A = 3.025×10^{5}, $\alpha=-5.039$, $E_{\mathrm{a}}=9.891\times10^{-20}$ and k_{b} being the Boltzmann constant. ΔT_{j} is the junction temperature variation, and T_{jm} is the average junction temperature. It should be noted that different lifetime models may lead to different evaluated results. To compare the fixed frequency and the proposed adaptive scheme in this paper, the selection of different lifetime models does not affect the relative results. More details about different lifetime models can refer to [23].

At the meantime, the accumulated damage is evaluated as

$$D=\sum_{i=1}^{k}\frac{n_i}{N_{\mathrm{f}i}} \tag{16}$$

where D represents the accumulated damage index; k denotes the total number of different thermal stress levels. n_i represents the cycle number for a specific stress type (e.g., ΔT_{j}); $N_{\mathrm{f}i}$ represents the cycle-to-failure for the i^{th} stress type. Fig. 9 demonstrates that the adaptive frequency scheme causes less damage (e.g., 12%) than the fixed frequency scheme with a longer power device lifetime expectation.

V. EXPERIMENTAL VALIDATION

To validate the effectiveness of the proposed adaptive carrier frequency control, a series of experiments are carried out on the three-phase MMC prototype shown in Fig. 10. It consists of four SMs per arm, each equipped with an IGBT module F4-50R12KS4, 400 V capacitors, and the bleeding resistor to safely discharge SM capacitor. The detailed parameters are summarized in Table III. The target of the adaptive frequency scheme is to keep the ac current THD within 5% and the SM voltage ripple within 10%.

A. Output Current THD and SM Voltage Ripple

Fig. 11 compares the output current THD of the conventional fixed frequency scheme and the proposed adaptive frequency scheme. With a fixed carrier frequency (e.g., 3045 Hz), the output current THD is decreased from around 5% to 1.86% with the increase of the power loading. By contrast, by applying the proposed approach, the current THD is always

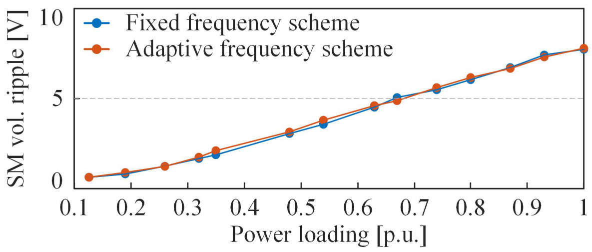

Fig. 13. SM voltage ripple (half peak-to-peak value).

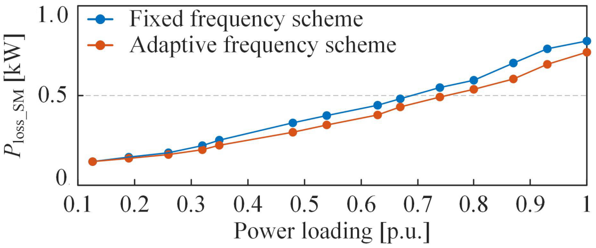

Fig. 14. Experimental power loss results of all 24 SMs in the three-phase MMC system.

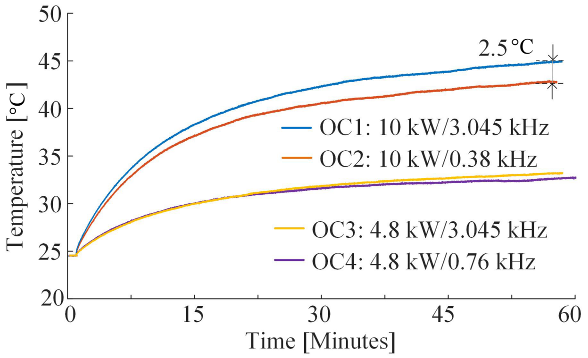

Fig. 15. Experimental results: thermal stress on S_2 under four operating conditions.

maintained at around 5% by the varied carrier frequency for different power levels. The corresponding current waveforms are provided in Fig. 12. Meanwhile, as shown in Fig. 13, the measured SM voltage ripples exhibit no significant deviation with the different carrier frequency approaches, which gradually increase with the rising power level but still remain within the required ripple range. These findings are in agreement with the aforementioned analytical and simulation results.

B. Power Loss and Thermal Stress Measurements

A power analyzer (PPA4500) is used to measure the actual power loss of the SM, as presented in Fig. 14. It is clear that the proposed scheme reduces the power losses by approximately 10%. This reduction in power losses is expected to enhance the reliability of the power semiconductor devices.

The impact of the power loading and arm carrier frequency on thermal stress of power devices are measured under four operating conditions: OC1: 10 kW/3.045 kHz, OC2: 10 kW/0.38 kHz, OC3: 4.8 kW/3.045 kHz, and OC4: 4.8 kW/0.76 kHz. The temperature is measured by an optical fiber. S_2 is taken as the example for illustration. Fig. 14 shows junction temperatures of S_2 after one-hour continuous operation under four conditions. For the load condition of P_{load} =10 kW, the junction temperature of S_2 reaches around 45 °C and 42.5 °C for the fixed and adaptive carrier frequency schemes. As a rule of thumb [24], 2.5 °C junction temperature decrease, shown in Fig. 14, will improve the lifetime of the SM by roughly 30%. When the power level is lower, i.e., P_{load} = 4.8 kW, the temperature difference between the fixed frequency and adaptive frequency control is not apparent. That is caused by the thermal cross-coupling effects which has been systematically investigated in [3]. However, the apparent power loss reduction is beneficial for the system efficiency.

VI. CONCLUSION

An adaptive carrier frequency scheme is proposed in this paper to reduce the power losses of the MMC under variable operating conditions. The carrier frequency is adjusted flexibly under different power loadings to achieve the tradeoff between achieving performance metrics such as THD and SM voltage ripple, and minimizing power losses. Through this study, we have the following conclusions:

- In contrast to existed active thermal control relying on accurate power loss and thermal models, the proposed approach focuses on manipulating a power loss-related variable (the carrier frequency). This makes the proposed method more practical and tangible for power electronics converters in real-world applications.
- By the established analytical model of the THD and the capacitor voltage ripple, the THD requirement takes precedence in selecting the carrier frequency.
- The effectiveness of the proposed scheme has been validated through comprehensive simulations on a 15-MVA MMC system and experimental measurements on a 15-kW prototype. The results demonstrate significant reductions in power losses and thermal stresses, contributing to improved reliability.

REFERENCE

[1] M. A. Perez, S. Bernet, J. Rodriguez, S. Kouro, and R. Lizana, “Circuit topologies, modeling, control schemes, and applications of modular multilevel converters,” in *IEEE Transactions on Power Electronics*, vol. 30, no. 1, pp. 4–17, Jan. 2015.

[2] D. Karwatzki and A. Mertens, “Generalized control approach for a class of modular multilevel converter topologies,” in *IEEE Transactions on Power Electronics*, vol. 33, no. 4, pp. 2888–2900, Apr. 2018.

[3] Y. Zhang, H. Wang, Z. Wang, F. Blaabjerg, and M. Saeedifard, “Mission profile-based system-level reliability prediction method for modular multilevel converters,” in *IEEE Transactions on Power Electronics*, vol. 35, no. 7, pp. 6916–6930, Jul. 2020.

[4] Y. Zhang, H. Wang, Z. Wang, Y. Yang, and F. Blaabjerg, “Simplified

thermal modeling for IGBT modules with periodic power loss profiles in modular multilevel converters," in *IEEE Transactions on Industrial Electronics*, vol. 66, no. 3, pp. 2323–2332, Mar. 2019.

[5] F. Hahn, M. Andresen, G. Buticchi, and M. Liserre, "Thermal analysis and balancing for modular multilevel converters in HVDC applications," in *IEEE Transactions on Power Electronics*, vol. 33, no. 3, pp. 1985–1996, Mar. 2018.

[6] H. Mao, H. Jiang, L. Ran, J. Hu, G. Qiu, J. Wei, H. Chen, X. Zhong, N. Xiao, L. Wang, *et al*. "An asymmetrical power module design for modular multilevel converter with unidirectional power flow," in *IEEE Transactions on Power Electronics*, vol. 38, no. 1, pp. 1092–1103, Jan. 2023.

[7] B. Xu, L. Tu, S. Gong, G. Wang, C. Gao, and Z. He, "Component-level semiconductor loss balancing for IGBT based high power MMC through insertion index modification," in *IEEE Transactions on Power Electronics*, vol. 37, no. 12, pp. 14781–14794, Dec. 2022.

[8] Z. Wang, H. Wang, Y. Zhang, and F. Blaabjerg, "Balanced conduction loss distribution among SMs in modular multilevel converters," in *2018 International Power Electronics Conference (IPEC-Niigata 2018 -ECCE Asia)*, Niigata, Japan, 2018, pp. 3123–3128.

[9] H. Qiu, J. Wang, P. Tu, and Y. Tang, "Device-level loss balancing control for modular multilevel converters," in *IEEE Transactions on Power Electronics*, vol. 36, no. 4, pp. 4778–4790, Apr. 2021.

[10] Y. Zhang, H. Wang, Z. Wang, and F. Blaabjerg, "Computational-efficient thermal estimation for IGBT modules under periodic power loss profiles in modular multilevel converters," in *IEEE Transactions on Industry Applications*, vol. 55, no. 5, pp. 4984–4992, Sept.-Oct. 2019.

[11] H. Li, F. Deng, J. Zhao, J. Tian, Y. Lu, and G. Li, "Variable sampling frequency-based SM power loss balancing control for MMCs with bypassed faulty SMs," in *IEEE Transactions on Power Electronics*, vol. 38, no. 7, pp. 9006–9018, Jul. 2023.

[12] Y. Zhang, H. Wang, Z. Wang, Y. Yang, and F. Blaabjerg, "A simplification method for power device thermal modeling with quantitative error analysis," in *IEEE Journal of Emerging and Selected Topics in Power Electronics*, vol. 7, no. 3, pp. 1649–1658, Sept. 2019.

[13] B. Li, Y. Zhang, D. Xu, and R. Yang, "Start-up control with constant precharge current for the modular multilevel converter," in *2014 IEEE 23rd International Symposium on Industrial Electronics (ISIE)*, Istanbul, 2014, pp. 673–676.

[14] X. Li, Q. Song, W. Liu, S. Xu, Z. Zhu, and X. Li, "Performance analysis and optimization of circulating current control for modular multilevel converter," in *IEEE Transactions on Industrial Electronics*, vol. 63, no. 2, pp. 716–727, Feb. 2016.

[15] R. Chakraborty and A. Dey, "Circulating current control of modular multilevel converter with reduced conduction loss for medium-voltage applications," in *IEEE Transactions on Industrial Electronics*, vol. 68, no. 10, pp. 9014–9023, Oct. 2021.

[16] D. Ronanki and S. S. Williamson, "Device loading and reliability analysis of modular multilevel converters with circulating current control and common-mode voltage injection," in *IEEE Journal of Emerging and Selected Topics in Power Electronics*, vol. 7, no. 3, pp. 1815–1823, Sept. 2019.

[17] B. Li, R. Yang, D. Xu, G. Wang, W. Wang, and D. Xu, "Analysis of the phase-shifted carrier modulation for modular multilevel converters," in *IEEE Transactions on Power Electronics*, vol. 30, no. 1, pp. 297–310, Jan. 2015.

[18] S. Lu, L. Yuan, K. Li, and Z. Zhao, "An improved phase-shifted carrier modulation scheme for a hybrid modular multilevel converter," in *IEEE Transactions on Power Electronics*, vol. 32, no. 1, pp. 81–97, Jan. 2017.

[19] C. Wang, L. Zhang, L. Xiao, F. Wu, X. Zheng, and H. Jiang, "Analysis and suppression of the frequency-decrease effect in the capacitor voltage related to the low modulation frequency ratio in an MMC system," in *IEEE Transactions on Power Electronics*, vol. 35, no. 9, pp. 9119–9132, Sept. 2020.

[20] P. Zhang, M. Saeedifard, O. C. Onar, Q. Yang, and C. Cai, "A field enhancement integration design featuring misalignment tolerance for wireless EV charging using LCL topology," in *IEEE Transactions on Power Electronics*, vol. 36, no. 4, pp. 3852–3867, Apr. 2021.

[21] S. Chattopadhyay, M. Mitra, and S. Sengupta, "Electric power quality," in *Electric Power Quality, Springer*, 2011, pp. 5–12.

[22] F. Sasongko, K. Sekiguchi, K. Oguma, M. Hagiwara, and H. Akagi, "Theory and experiment on an optimal carrier frequency of a modular multilevel cascade converter with phase-shifted PWM," in *IEEE Transactions on Power Electronics*, vol. 31, no. 5, pp. 3456–3471, May 2016.

[23] Y. Zhang, H. Wang, Z. Wang, Y. Yang, and F. Blaabjerg, "Impact of lifetime model selections on the reliability prediction of IGBT modules in modular multilevel converters," in *2017 IEEE Energy Conversion Congress and Exposition (ECCE)*, Cincinnati, OH, USA, 2017, pp. 4202–4207.

[24] N. -C. Sintamarean, F. Blaabjerg, H. Wang, F. Iannuzzo, and P. de Place Rimmen, "Reliability oriented design tool for the new generation of grid connected PV-inverters," in *IEEE Transactions on Power Electronics*, vol. 30, no. 5, pp. 2635–2644, May 2015.

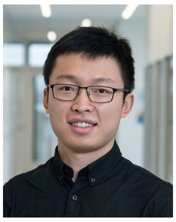

Yi Zhang received the B.S. and M.S. degrees from Harbin Institute of Technology, China, in 2014 and 2016, respectively, and the Ph.D. degree from Aalborg University, Denmark, in 2020. All degrees are in electrical engineering. He is currently an Assistant Professor with Aalborg University, Denmark. During 2020–2023, he was affiliated with multiple institutions as a postdoctoral researcher with the support of the Danish Research Council for Independent Research, including RWTH-Aachen University, Germany, Swiss Federal Institute of Technology Lausanne, Switzerland, and Massachusetts Institute of Technology, USA. He was also a visiting scholar with Georgia Institute of Technology, USA, in 2018. His research interests include the reliability of power electronics. Dr. Zhang received the First Place Prize Paper Award of the *IEEE Transactions on Power Electronics* in 2021, and the IEEE Power Electronics Society Ph.D. Thesis Award in 2020.

Yaqian Zhang received the B.S. degree from University of Electronic Science and Technology of China, Chengdu, China, in 2016, and the Ph.D. degree from Southeast University, Nanjing, China, in 2023. During 2021–2022, she was a visiting student in Aalborg University. She is currently a lecturer in Southeast University. Her research focuses on high-voltage power electronic converters including modular multilevel converter and the solidstate transformer.

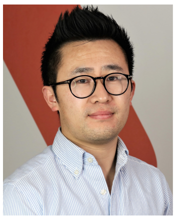

Zhongxu Wang received Ph.D. degree in Electrical Engineering from Aalborg University, Denmark, in 2019 and was a visiting researcher with the Energy Futures Lab at Imperial College London, UK, in 2018. He is currently a principle reliability engineer and project manager with Nexperia UK since 2021, before which he was with Dynex Semiconductor UK as a senior R&D engineer since 2020, with research focusing on the reliability of power semiconductors, including IGBT, WBG devices and power modules.